Technical Notes

TECHNICAL NOTES are short manuscripts describing new developments or important results of a preliminary nature. These Notes should not exceed 2500 words (where a figure or table counts as 200 words). Following informal review by the Editors, they may be published within a few months of the date of receipt. Style requirements are the same as for regular contributions (see inside back cover).

Suppressing Restricted Shock Separation in a Subscale Rocket Nozzle Using Contour Geometry

K. Schomberg* and J. Olsen†
UNSW Australia,
Sydney, NSW 2052, Australia
A. Neely‡
UNSW Canberra,
Canberra, ACT 2600, Australia
and
G. Doig§
California Polytechnic State University,
San Luis Obispo, CA 93407

DOI: 10.2514/1.B36059

Nomenclature

C_F	=	thrust coefficient at low-altitude operating conditions
C_{F0}	=	thrust coefficient at adapted conditions
$C_{F\infty}$	=	thrust coefficient at vacuum conditions
P	=	static pressure, Pa
P_a	=	ambient pressure, Pa
r	=	radius, m
x	=	streamwise distance, m
y	=	spanwise distance, m
θ	=	angle, deg

Subscripts

i	=	arbitrary contour point i
j	=	arbitrary contour point j
k	=	arbitrary contour point k
m	=	nozzle inflection point
n	=	nozzle exit point
t	=	nozzle throat

Presented as Paper 2015-4220 at the 51st AIAA/SAE/ASEE Joint Propulsion Conference, Orlando, FL, 27–29 July 2015; received 27 October 2015; revision received 27 April 2016; accepted for publication 2 May 2016; published online 18 July 2016.

*Ph.D. Candidate, School of Mechanical and Manufacturing Engineering; kyll.schomberg@unsw.edu.au. Student Member AIAA.
†Lecturer, School of Mechanical and Manufacturing Engineering.
‡Associate Professor, School of Engineering and Information Technology. Associate Fellow AIAA.
§Assistant Professor, Co-Appointment: Adjunct Lecturer, Aerospace Engineering Department; also UNSW Australia. Senior Member AIAA.

I. Introduction

THE use of a thrust-optimized contour (TOC) [1,2] for the supersonic nozzle in a rocket engine will inherently maximize the propulsive efficiency and payload capacity of the entire launch system. A TOC can be approximated using a skewed parabola, commonly referred to as a thrust-optimized parabola (TOP) [3], and the TOP contour can be manipulated to avoid undesirable flow separation during low-altitude operation by increasing the static wall pressure at the expense of thrust (approximately 0.1–0.2%) [4]. For this reason, a TOP design is often used in nozzles with a high area ratio, such as those used in the Vulcain [5] and Vulcain 2 [6] core-stage engines, and suggests that ensuring full-flowing operation at low-altitude conditions can be considered a nozzle design requirement. Unfortunately, any thrust-optimized nozzle may excite an undesirable shift between a "free" shock separation (FSS) and "restricted" shock separation (RSS) mode during engine startup and shutdown [7].

The shift between an FSS and an RSS flow regime was first noticed during operation of the high-area-ratio J2-S engine, and the RSS condition consequently was deemed responsible for inducing high structural loading to the nozzle walls [8]. However, it was later found that the highest levels of side loading were, in fact, caused by the transition process to and from the RSS flow condition, as opposed to the RSS phenomenon itself [5,9,10]. Because the precise flow mechanisms that drive the transition to and from the RSS condition are still not fully understood [11], the structural loading that occurs as a result of RSS appears to currently be accepted as a design consideration in core-stage rocket nozzles [6].

A nozzle contour that was capable of suppressing the RSS flow condition itself would inherently prevent the transition to and from RSS and, therefore, decrease the structural loading that occurs during these transition phases. For a net benefit to be realized, the resulting nozzle must produce an equal or greater thrust coefficient compared to the existing design, as well as avoid flow separation during low-altitude operation. In this paper, a set of equivalent thrust-optimized nozzle contours have been produced using an arc-based design method to determine if the suppression of RSS could be achieved by manipulating the contour geometry. The subscale Volvo S1 TOP nozzle that was designed by Volvo Aero Corporation (now GKN Aerospace Engine Systems) was selected as the test case due to the availability of experimental data that captures the transition from FSS to RSS [5,9] and to ensure that a positive result may be applicable to a full-scale rocket engine, because this nozzle has been shown to possess equivalent flow characteristics to the core-stage Vulcain engine nozzle [5].

II. Numerical Model

A numerical approach was used to evaluate the separation behavior and thrust coefficient of the Volvo S1 TOP nozzle and all arc-based nozzle variants considered in the work. The existing Volvo S1 contour geometry was directly replicated to represent the baseline design [3,5]. Because of the long test times used to cover the startup process in the existing Volvo S1 experiments (>40 s), all numerical results were generated from the steady Reynolds-averaged form of the Navier–Stokes equations using the commercially available ANSYS Fluent 14.5 finite volume code. An implicit, pressure-based, axisymmetric solver was used, and all terms discretized in space using second-order upwind schemes. Air behaving as an ideal gas was selected as the working fluid and viscosity modeled by a three-

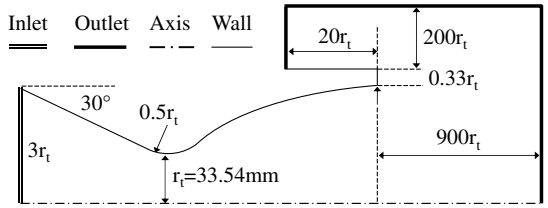

Fig. 1 Numerical domain, including inlet and downstream exhaust region (not to scale).

coefficient Sutherland approximation [12]. The Reynolds number based on the nozzle throat diameter varied between 5.76×10^6 and 28.8×10^6 as the inlet stagnation pressure was increased from 1 to 5 MPa, and the inlet stagnation temperature was maintained at 450 K, consistent with the experimental conditions [5,9].

The startup conditions were modeled using a pressure stepping process, starting from an inlet to outlet pressure ratio (PR) of 10 and finishing at 50, which corresponded to the low-altitude operation of the Volvo S1 nozzle, where full-flowing conditions could be expected [5]. The PR was increased by increments of one between a PR of 10 and 30 and two between a PR of 30 and 50. Comparatively, the outlet pressure was reduced to model the adapted (PR = 350) and vacuum conditions (PR $\rightarrow \infty$) once the initial PR of 50 was reached. The thrust coefficient was calculated from the flow conditions at the nozzle exit plane, and the dimensions of the downstream exhaust region were selected to ensure the domain boundary did not affect the solution. The numerical domain, including dimensions of the inlet and downstream exhaust regions, is shown in Fig. 1. The numerical model was verified by demonstrating independence of spatial discretization, as well as determining the effect of the chosen turbulence closure model. Validation of the model was achieved by comparing the static pressure distribution with the existing experimental results. A comprehensive account of the model verification and validation process is given in [13].

The spatial discretization of the domain was completed using quadrilateral elements, such that a nondimensional wall distance (y^+) of less than 1 was maintained in all models. Refinement of the grid was focused primarily on the nozzle region and a grid convergence study conducted at three levels using a coarse, standard, and fine grid, comprised of approximately 5×10^4, 8×10^4, and 15×10^4 elements, respectively. The coarse grid indicated a greater streamwise distance before the second recirculation zone at RSS conditions and underpredicted the pressure inflection in the initial separated zone compared to the experiment. The standard level of grid refinement was therefore accepted and used to produce all results. In addition, the thrust coefficients at low-altitude (PR = 50), adapted (PR = 350), and vacuum (PR $\rightarrow \infty$) conditions were calculated to determine the effect of grid density on thrust. However, no variation in thrust was observed relative to grid density at all conditions to an accuracy of 0.001 (<0.1%).

Verification of the turbulence model was assessed by comparing the Spalart–Allmaras (SA) model [14] and Menter's shear stress transport (SST) model [15] to an inviscid solution. The thrust coefficient was overpredicted by 0.42% in the inviscid solution under all conditions, which was expected due to the influence of the boundary layer on thrust. Comparatively, the difference in thrust between the SA and SST solutions was less than 0.1% at all conditions. The point of initial separation in the SST solution was predicted to be upstream of the experimental value by appoximately 7.5%, whereas the variation in the SA model was less than 1% under both FSS and RSS conditions. As a result, the SA model was selected for use in all future models.

III. Contour Variation

All variants of the Volvo S1 nozzle contour were generated using a design method that is based on a finite series of circular arcs [16,17], using the notation given in Fig. 2. In all variants, the spanwise and streamwise dimensions of the nozzle were kept consistent with the existing Volvo S1 design to facilitate a direct comparison between configurations. This can be achieved by considering the total nozzle

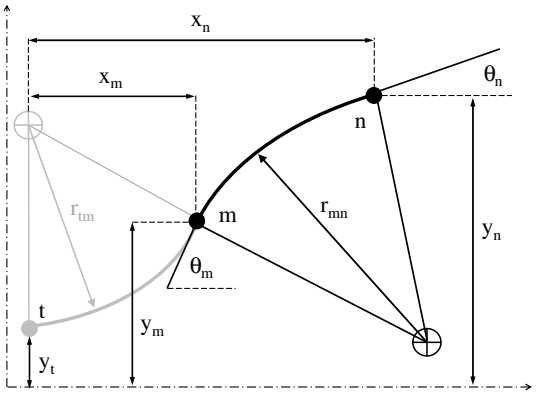

Fig. 2 Representation of a turning curve arc segment as two right-angled triangles.

dimensions as a right-angled triangle and assuming the tangent of the resulting angle will approach the angle itself. Variation of the contour is then determined by the selected inflection and exit angle, as shown in Eq. (1).

$$\frac{y_{mn}}{x_{mn}} = \tan\,\theta_{mn} \approx \theta_{mn} \approx \frac{\theta_m + \theta_n}{2} \tag{1}$$

For the case of the Volvo S1 nozzle, an angle sum of 37.5 was used to both replicate the nozzle dimensions and to eliminate the effect of the expansion curve radius, which was maintained at half the throat radius for similarity with the existing design [5]. The nozzle area ratio and throat radius in all variants were kept consistent with the existing Volvo S1 nozzle at a valuea of 20 and 33.54 mm, respectively [5], and a single arc segment was used for the turning curve in each nozzle variant. Five equivalent nozzle contours were generated using selected integer values for the ratio of inflection to exit angle. The geometric information regarding each equivalent nozzle contour is given in Table 1.

All equivalent nozzle contours were evaluated with respect to flow behavior and predicted thrust. Static pressure distributions along the divergence wall at PRs of 14, 18, 24, 30, 38, and 50 were selected to identify if the transition between the FSS and RSS flow regimes occurred during the simulated startup process of the nozzle (Fig. 3). The thrust coefficient was calculated for low-altitude, adapted (PR = 350), and vacuum (PR $\rightarrow \infty$) operating conditions (Table 2) to ensure that the suppression of RSS was not accompanied by an adverse effect on predicted thrust.

The variation between the Volvo S1 and KS9 configurations was minimal, which was to be expected given the similarity in contour geometry. In both cases there was evidence that the RSS separation bubble had moved downstream of the nozzle exit at a PR of 30, consistent with the expected behavior of the Volvo S1 nozzle [5]. The RSS flow phenomenon was also observed in the KS6 configuration. Comparatively, the RSS flow condition was suppressed in the KS4, KS3, and KS2 nozzle configurations, where the point of initial separation for all PRs was shown to move upstream as the ratio of inflection to exit angle was reduced. Evidence of separated flow at low-altitude conditions was observed in the KS4, KS3, and KS2 contours, where the point of separation was observed to be 2, 4, and 12% upstream of the nozzle exit respectively.

The predicted thrust coefficient was equal in the KS9 and Volvo S1 nozzles at all operating conditions, whereas all other nozzle configurations indicated an increase in predicted thrust at adapted

Table 1 Inflection and exit angles in each equivalent nozzle contour

Variable	Volvo S1	KS9	KS6	KS4	KS3	KS2
θ_m/θ_n	— —	9	6	4	3	2
θ_m	35.0	33.75	32.14	30.0	28.125	25.0
θ_n	4.0	3.75	5.36	7.5	9.375	12.5
r_{mn}	— —	$20.4r_t$	$22.8r_t$	$27.2r_t$	$32.6r_t$	$49.0r_t$

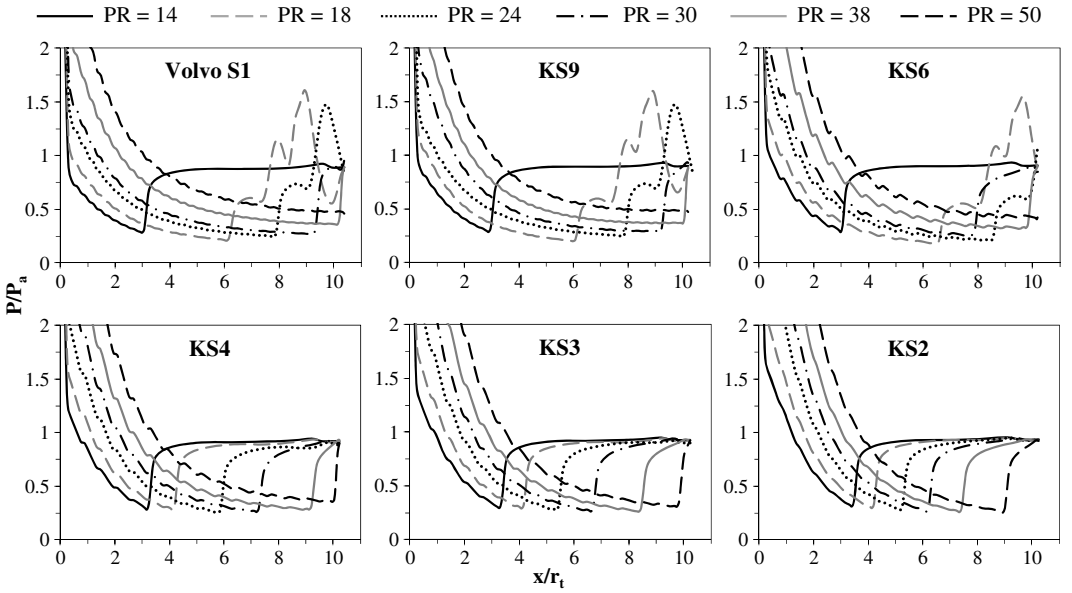

Fig. 3 Static pressure distributions of the equivalent nozzle contours during startup conditions.

and vacuum operating conditions. A decrease in the thrust coefficient of 0.23% was observed in the KS2 configuration at low-altitude operating conditions, which was predominantly a function of flow separation occurring considerably upstream of the nozzle exit. The potential increase in thrust at each operating condition ranged between 0.39 and 0.43% compared with the existing design, and it was particularly significant in this case, considering that the highest performing configurations also suppressed the transition to an RSS flow condition. However, assuming that unseparated flow at low-altitude operating conditions was a design specification, none of the equivalent nozzle contours represented a valid alternative to the existing Volvo S1 design. Additional consideration of the equivalent nozzle configurations was therefore desirable and has been addressed by the use of two arc segments in the turning curve of the KS3 nozzle.

IV. Turning Curve Manipulation

The design of a dual-segment turning curve nozzle follows similar principles to a single curve arc-based nozzle; however, the notation used in Fig. 2 is insufficient for the design of a dual-segment nozzle and therefore was replaced in the notation used in Fig. 4. If the expansion curve is retained, two possible configuration types can be defined for a dual-segment turning curve. These are best defined by comparing the contour angle at the nozzle exit to the existing exit angle, which is ultimately determined by the ratio of the turning curve segment radii. A detailed account of the design process in a dual-segment turning curve nozzle is given in [13].

Four nozzle variants of the KS3 configuration were generated, and the geometric parameter values are given in Table 3. Two variants were generated from ratios of curve segment radii that were less than one and two variants from ratios greater than one. These values were chosen to represent a considerable range of the geometric design limits and to ensure that the predominant effects of introducing a second arc segment into the turning curve of an arc-based nozzle were identified.

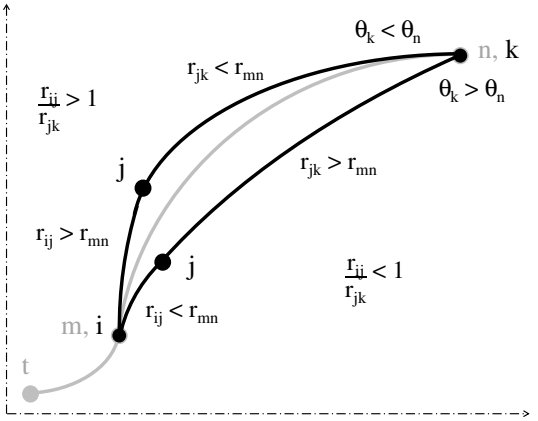

Fig. 4 Notation for a dual-segment turning curve nozzle contour.

The static wall pressure distribution and predicted thrust coefficient in the KS3 variants are shown in Fig. 5 and Table 4, respectively.

The transition to RSS was avoided in all KS3 nozzle variants across the entire range of startup operating conditions, highlighting the influence of the expansion curve in this process. An upstream shift in the

Table 3 Dual-segment turning curve nozzle parameters for the KS3 configuration variants

Nozzle	KS3_1	KS3_2	KS3_3	KS3_4
θ_j	16.41	17.97	19.92	22.27
θ_k	14.06	10.94	7.031	2.344
r_{ij}	$26.1r_t$	$30.1r_t$	$37.3r_t$	$54.9r_t$
r_{jk}	$130r_t$	$43.4r_t$	$23.8r_t$	$15.4r_t$

Table 2 Predicted thrust coefficient in the equivalent nozzle contours

Nozzle	C_F	Δ%	C_{F0}	Δ%	$C_{F\infty}$	Δ%
Volvo S1	1.273	—	1.617	—	1.674	—
KS9	1.273	0.000	1.617	0.000	1.674	0.000
KS6	1.277	0.314	1.621	0.247	1.678	0.239
KS4	1.278	0.393	1.623	0.371	1.680	0.358
KS3	1.277	0.314	1.624	0.433	1.681	0.418
KS2	1.270	−0.236	1.622	0.309	1.680	0.358

Table 4 Predicted thrust coefficient in the KS3 nozzle variants

Nozzle	C_F	Δ%	C_{F0}	Δ%	$C_{F\infty}$	Δ%
Volvo S1	1.273	—	1.617	—	1.674	—
KS3_1	1.271	−0.157	1.624	0.433	1.681	0.418
KS3_2	1.275	0.157	1.625	0.495	1.682	0.478
KS3	1.277	0.314	1.624	0.433	1.681	0.418
KS3_3	1.278	0.393	1.623	0.371	1.680	0.358
KS3_4	1.273	0.000	1.616	−0.062	1.674	0.000

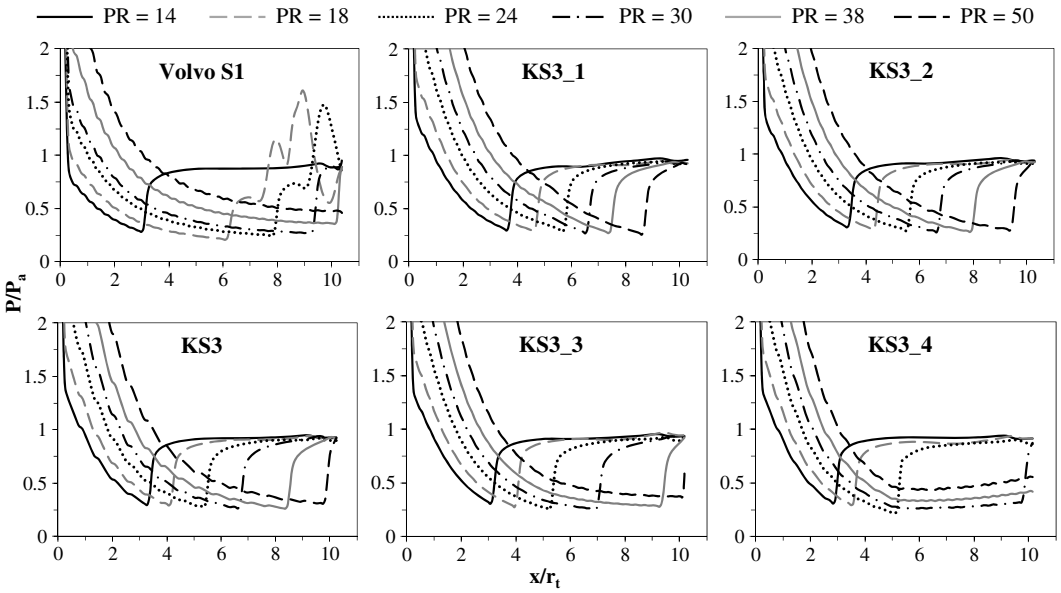

Fig. 5 Static pressure distributions of KS3 nozzle variants during startup conditions.

separation point at low-altitude operating conditions was observed in both the KS3_1 and KS3_2 variants, whereas the separation point was shifted to within 0.90% of the nozzle exit in the KS3_3 variant and led to an adverse pressure gradient and early full-flowing condition in the KS3_4 configuration. The result suggested that unseparated flow at initial conditions independent of RSS could be achieved in a dual-segment turning curve variant of the KS3 configuration.

An upstream shift in the separation point that was observed in the KS3_1 and KS3_2 variants resulted in a reduction in thrust at low-altitude conditions due to the greater influence of the separated region. Comparatively, a downstream shift in the separation point in the KS3_3 configuration caused an increase in the predicted thrust coefficient at low-altitude operating conditions. The adverse pressure gradient observed in the KS3_4 variant was responsible for reducing thrust to approximately equal that of the Volvo S1 nozzle. An increase of 0.05–0.06% in the adapted and vacuum thrust coefficient was predicted in the KS3_2 variant compared with the KS3 configuration, whereas a 0.06% decrease was predicted in the KS3_3 variant under these conditions.

V. Conclusion

Suppression of the RSS flow phenomenon during the numerically simulated startup process of a subscale rocket nozzle has been achieved. All equivalent nozzle contours returned an equal or greater thrust coefficient relative to the existing design (Volvo S1), where three of these configurations also avoided the RSS flow condition (KS4, KS3, and KS2). However, the suppression of RSS in all equivalent nozzle contours was accompanied by separated flow at low-altitude operating conditions, and further manipulation of the nozzle contour was considered by representing the turning curve as two arc segments. The use of a dual-segment turning curve nozzle presented a feasible design method for the suppression of RSS that was coupled with a likely increase in predicted thrust coefficient of 0.36–0.39% relative to the Volvo S1 nozzle at all operating conditions. Although comparison in this case was restricted to a single subscale TOP nozzle, the net benefit in terms of predicted thrust and the suppression of RSS in an equivalent arc-based nozzle configuration may increase the performance and reliability of a core-stage rocket engine, and should be investigated further.

References

[1] Rao, G., "Exhaust Nozzle Contour for Optimum Thrust," *Jet Propulsion*, Vol. 28, No. 6, 1958, pp. 377–382. doi:10.2514/8.7324

[2] Guderley, G., and Hantsch, E., "Beste Formen für Achsensymmetrische Uberschallschubdusen," *Zeitschrift für Flugwissenschaften*, Vol. 3, No. 9, 1955, pp. 305–313.

[3] Rao, G., "Approximation of Optimum Thrust Nozzle Contour," *ARS Journal*, Vol. 30, No. 6, 1960, p. 561.

[4] Chen, J., and Freeman, J., "Thrust Chamber Performance Using Navier–Stokes Solution," NASA TR-D951729, 1984.

[5] Östlund, J., "Flow Processes in Rocket Engine Nozzles with Focus on Flow Separation and Side-Loads," Ph.D. Dissertation, Royal Inst. Technol., Stockholm, Sweden, 2002.

[6] Vuillermoz, P., Weiland, C., Hagemann, G., Aupoix, B., Grosdemange, H., and Bigert, M., "Nozzle Design and Optimization," *Progress in Astronautics and Aeronautics: Liquid Rocket Thrust Chambers*, AIAA, Reston, VA, 2004, pp. 469–492.

[7] Frey, M., and Hagemann, G., "Restricted Shock Separation in Rocket Nozzles," *Journal of Propulsion and Power*, Vol. 16, No. 3, 2000, pp. 478–484. doi:10.2514/2.5593

[8] Nave, L., and Coffey, G., "Sea Level Side Loads in High-Area-Ratio Rocket Engines," *Ninth Joint Propulsion Conference*, AIAA Paper 1973-1284, 1973.

[9] Mattsson, J., Hogmann, U., and Torngren, L., "A Sub Scale Test Programme on Investigation of Flow Separation and Side Loads in Rocket Nozzles," *Third European Symposium on Aerothermodynamics for Space Vehicles*, European Space Agency, Noordwijk, The Netherlands, 1999, pp. 373–378.

[10] Wang, T., "Transient Three-Dimensional Startup Side Load Analysis of a Regeneratively Cooled Nozzle," *Shock Waves*, Vol. 19, No. 3, 2009, pp. 251–264. doi:10.1007/s00193-009-0201-2

[11] Hadjadj, A., and Onofri, M., "Nozzle Flow Separation," *Shock Waves*, Vol. 19, No. 3, 2009, pp. 163–169. doi:10.1007/s00193-009-0209-7

[12] Sutherland, W., "The Viscosity of Gases and Molecular Force," *Philosophical Magazine*, Vol. 36, No. 223, 1893, pp. 507–531. doi:10.1080/14786449308620508

[13] Schomberg, K., Olsen, J., Neely, A., and Doig, G., "Suppressing Restricted Shock Separation in Thrust-Optimized Rocket Nozzles Using Contour Geometry," *51st Joint Propulsion Conference*, AIAA Paper 2015-4220, 2015.

[14] Spalart, P., and Allmaras, S., "A One-Equation Turbulence Model for Aerodynamic Flows," *La Recherche Aerospatiale*, Vol. 1, No. 5, 1992, pp. 5–21.

[15] Menter, F., "Two Equation Eddy-Viscosity Turbulence Models for Engineering Applications," *AIAA Journal*, Vol. 32, No. 8, 1994, pp. 1598–1605. doi:10.2514/3.12149

[16] Schomberg, K., Olsen, J., Neely, A., and Doig, G., "Design of an Arc-Based Thrust-Optimized Nozzle Contour," *Sixth European Conference for Aerospace Sciences*, Luciano Galfetti, Krakow, Poland, 2015, p. 43.

[17] Schomberg, K., Olsen, J., and Doig, G., "Design of High Area Nozzle Contours Using Circular Arcs," *Journal of Propulsion and Power*, Vol. 32, No. 1, 2016, pp. 188–195.

K. Frendi
Associate Editor